Mode-Locked Laser Array Monolithically Integrated with SOA and EA-Modulator

Lianping Hou, Mohsin Haji, Anthony E. Kelly, John M. Arnold, A. Catrina Bryce
School of Engineering, University of Glasgow, G12 8LT Glasgow, U.K.
lhou@elec.gla.ac.uk

Abstract: The monolithic integration of four 10 GHz multi-colored mode-locked lasers with a 4×1 MMI, a SOA and an electroabsorption modulator has been demonstrated. The lasers produce 2.49 ps $Sech^2$-pulses with TBP of 0.389.

OCIS codes: (140.4050) Mode-locked laser; (140.5960) Semiconductor lasers; (140.2010) Diode laser arrays

1. Introduction

An increasing number of channels in wavelength division multiplexing (WDM) systems are required due to the massive growth of internet traffic. Monolithic mode-locked DBR laser diode (MLDLD) arrays with simultaneous multichannel operation are a key component for optical code division multiple access (OCDMA) and optical time division multiple access (OTDM) systems [1]. Compared to hybrid integrated MLDLD array modules consisting of several discrete devices, monolithically integrated MLDLD arrays can potentially reduce system costs by simplifying optical alignment and packaging processes. The passive sections of the monolithic device require a wider bandgap than the active regions to reduce the direct interband absorption. Such bandgap engineering is usually obtained by selective etching and re-growth processes. In this work we use a simple, flexible and low-cost alternative technique- quantum well intermixing (QWI) in the fabrication of four 10 GHz 1.55-μm AlGaInAs/InP mode-locked DBR lasers with a monolithically integrated 4×1 multimode-interference (MMI) optical coupler, a semiconductor optical amplifier (SOA) and an electroabsorption modulator (EAM). QWI technology was used to blue-shift the bandgap of the passive sections (DBR, phase section, S-bend, and MMI section) relative to the active sections, i.e., gain, saturable absorber (SA) section, SOA and EAM sections. The DBR was optimally designed with third-order surface-etched Bragg gratings, moderate coupling efficiency ($\kappa \sim 65$/cm), low absorption and scattering losses [2].

2. Device structure and fabrication

The epitaxial structure is described in [3]. The fabricated monolithically integrated four-channel MLDLD array along with its dimensions is shown in Fig. 1. Separation between two adjacent lasers was set at 250 μm. The raised cosine S-bends are 1200-μm-long. These S-bend patterns avoid discontinuities in the radius of curvature and thus minimize mode mismatch loss [4]. The MMI coupler is 30-μm-wide and 526-μm-long. In order to reduce the reflectivity from the MMI coupler, we used a 45˚ tilt at each corner [5]. The SOA consists of a 300-μm-long straight waveguide, followed by a 300-μm-long curved waveguide, which extends to the 150-μm-long EAM section. The curvature is chosen in such a way, that the waveguide and the cleavage plane form an angle of 80˚. The tilt angle of the facet is then equal to 10˚ to reduce the optical reflectivity [6]. A 30-μm-long electrical isolation slot is used between the SOA and EAM sections. The MLDLD has a total length of 4365 μm and consists of a gain section (3010 μm), 70-μm-long SA, phase section (1100 μm) and a 140-μm-long 3rd-order DBR section. The period of the DBR varied from 734 to 740 nm for channel 1 to channel 4. A slot width of 180 nm was selected due to a trade-off between reduced scattering losses and fabrication feasibility, while still providing adequate reflectivity [2]. As a result of the high κ, the effective length of the DBR is about 55 μm, therefore the effective cavity length is estimated to be ~4280 μm. This value corresponds to a round-trip frequency of approximately 10 GHz. The fabrication processes are similar to that used in [7]. The only difference being the use of hydrogen silsesquioxane (HSQ) in the planarization of the ridge waveguide. The QWI process produced a bandgap shift of 100 nm in the passive sections. The gain, SA section, SOA, and EAM section did not exhibit any significant shift [7]. HSQ acted as both electron-beam lithography resist and dry etching hard-mask for the definition of a 2.5-μm-wide, 1.92-μm-high ridge waveguide and the 3rd order gratings using electron beam lithography and a CH_4:H_2:O_2 reactive ion etching (RIE) dry etching process. The 250-nm-thick contact layer was removed by wet etching from the electrical isolation areas, the S-bend and MMI regions in order to obtain electrical isolation and reduce the absorption loss.

3. Device performance

Pure 10 GHz mode-locking characteristics were observed for gain section currents, I_{gain}, between 110 mA to 240 mA and SA reverse bias voltage $|V_{SA}|$ of ≥ 2.0 V. Fig. 2(a) shows the typical gain section light-current (L-I)

characteristics from the EAM facet and the output power dependence on the SOA injection current (I_{SOA}) with all other sections unbiased. The threshold current with an unbiased absorber section was 74 mA. Kinks were observed on some L-I curves, especially when I_{SOA} was greater than 120 mA. These are caused by a thermal detuning of the gain and reflector sections. The SOA has a negligible effect on the output pulse quality, while it increases the output power by as much as 30 dB at I_{SOA}=200 mA. From the SOA ASE spectra at various I_{SOA}, we can see the gain ripple is less than 0.5dB even at I_{SOA}=200 mA, which is consistent with the expected theoretical optical reflectivity of less than 10^{-4} using a 10˚ tilt angle [6]. A direct current (DC) extinction ratio of > 15 dB at V_{EAM}= -4 V was achieved for all the four channels (see Fig.2 (b)).

Fig.3 (a) shows the lasing spectra of the four channels under the conditions stated in the caption. The spacing of the spectra is about 5nm. Fig.3 (b) shows the measured pulse width of channel 3 as a function of the I_{gain} for different SA biases with I_{DBR} = 0 mA, I_{SOA}=200 mA and the phase and EAM sections left floating. For all other channels, the results were similar. For a fixed I_{gain} value, as V_{SA} was increased, the pulse width reduced due to the exponentially decreasing absorber recovery times with increasing reverse bias. For all investigated V_{SA}, when I_{gain} was increased, the pulse width broadened due to chirp induced by self-phase modulation (SPM) [8]. The shortest pulse width was observed at I_{gain} = 118 mA, I_{DBR} = 0 mA, where the autocorrelation width of an isolated pulse was 3.84 ps, which deconvolves to 2.49 ps pulse duration assuming a $Sech^2$ pulse shape. The period of the emitted pulse train was 100 ps, corresponding to the radio frequency (RF) spectrum signal at 10 GHz (see Fig. 4). The optical spectrum was centered at 1561.3 nm with a 3 dB bandwidth of 1.27 nm and the measured peak reflectivity is ~47 %, which is in accordance with the coupling efficiency κ of 65/cm and loss coefficient of ~5/cm. The relatively low loss was due to the QWI, grating duty cycle optimization, HSQ passivation and planarization to the DBR. The time-bandwidth product of the pulse is equal to 0.389, which is nearly transform-limited (0.315 for $sech^2$ shape pulse).

Fig. 5 summarizes the dependence of the peak wavelength (W_p), pulse repetition frequency (F_r), pulse width and time-bandwidth product (TBP) on the DBR tuning current, where the total injection current to the gain sections and the absorber reverse bias were fixed at 120, 180, 240 mA and -3.0 V, respectively. The injection current to the SOA was 200 mA. For all investigated I_{gain}, the peak wavelengths initially experienced a quasi-continuous blue-shift when I_{DBR} was increased from 0 mA to 15 mA due to the carrier effect of band-filling. At higher DBR currents (greater than 15mA), the thermally induced red-shift began to dominate the carrier induced blue-shift, so that the peak wavelength experienced an overall red-shift (see Fig.5 (a)). W_p could also be tuned by varying the injection current to the phase section.

From Fig.5 (b), we note typical trends, i.e. for all investigated V_{SA} and for a fixed I_{gain}, F_r decreases with increasing I_{DBR}. A tuning range of about 28 MHz was obtained when I_{DBR} was varied from 0 mA to 20 mA when I_{gain}= 120 mA. The frequency reduction with increasing I_{DBR} was consistent with the increase in the effective length caused by the lower absorption loss [9]. On the other hand, for a fixed value of I_{DBR} and V_{SA}, the F_r decreases with increasing I_{gain}. These anomalously high frequency shifts are mainly caused by the detuning of the cavity roundtrip frequency by gain/absorber saturation effects [10]. A tuning range of about 60 MHz was obtained when the I_{gain} varied from 120 mA to 240 mA for I_{DBR} = 0 mA. Tuning of the F_r could also be achieved by varying the V_{SA} or the injection current to the phase section. All the four channels were able to mode lock at the same F_r, making this device highly suitable for OTDMA and OCDMA applications.

From Fig.5 (c), we see that for a fixed I_{DBR}, as I_{gain} increases, the pulse width broadened due to chirp induced by SPM [8]. For the I_{gain}=120 mA case, as I_{DBR} increased, the TBP initially increased and then stabilized at around 0.49, which is very close to the transform-limited value. For I_{gain}=180, 240 mA cases, the TBP initially decreased and then stabilized at 0.6 and 1.0 respectively (see Fig.5 (d)), which is somewhat larger than the transform-limited value. This is due to SPM in the gain section [8].

4. Conclusion

In conclusion, for the first time we have fabricated four 10 GHz 1.55- μm AlGaInAs/InP mode-locked surface-etched DBR lasers monolithically integrated with a 4×1 MMI optical coupler, a SOA and an EAM using the very simple QWI technology, which has the advantage of eliminating crystal re-growth processes that are required in traditional methods. The mode-locked operation results show that the device has great potential for use in wavelength-hopping/time-spreading optical systems and applications.

The authors would like to acknowledge the financial support from EPSRC (project EP/E065112/1–*High Power, High Frequency Mode-locked Semiconductor Lasers*) and the technical staff of JWNC at the University of Glasgow.

References

[1] W. Lee et al., "Synchronized mode-locked semiconductor lasers and applications in Coherent Communications," J. Light-wave Technol., **26**, 908-921(2008).

[2] L. Hou et al., "Monolithic 40 GHz passively mode-locked AlGaInAs/InP 1.55 μm MQW laser with surface-etched distributed Bragg reflector," IEEE Photon. Technol. Lett., **22**, 1503-1505(2010).
[3] L. Hou et al., "Subpicosecond pulse generation at quasi-40-GHz using a passively mode locked AlGaInAs/InP 1.55 μm strained quantum well laser," IEEE Photon. Technol. Lett., **21**, 1731-1733(2009).
[4] W. J. Minford et al., "Low-Loss Ti : Li NbO3 waveguide bends at λ= 1.3μm," IEEE J. Quantum Electron., **18**, 1802-1806 (1982).
[5] R. Hanfoug et al., "Reduced reflections from multimode interference couplers," Electron. Lett. **42**, 465(2006).
[6] A.J. Collar et al., "Low residual reflectivity of angled-facet semiconductor laser amplifiers," IEEE Photon. Technol. Lett., **2**, 553–555(1990).
[7] L. Hou et al., "Monolithic 45-GHz mode-locked surface-etched DBR laser using quantum-well intermixing technology," IEEE Photon. Technol. Lett., **22**, 1039-1041(2010).
[8] G. P. Agrawal et al., "Self-phase modulation and spectral broadening of optical pulses in semiconductor laser amplifiers," IEEE J. Quantum Electron., **25**, 2297–2306(1989).
[9] I. Ogura et al., "Precise operation-frequency control of monolithic mode-locked laser diodes for high-speed optical communication and all-optical signal processing," Opt. Quantum Electron., **33**, 709–725(2001).
[10]S. Arahira et al., "Repetition–frequency tuning of monolithic passively mode-locked semiconductor lasers with integrated extended cavities," IEEE J. Quantum Electron., **33**, 255–264(1997).

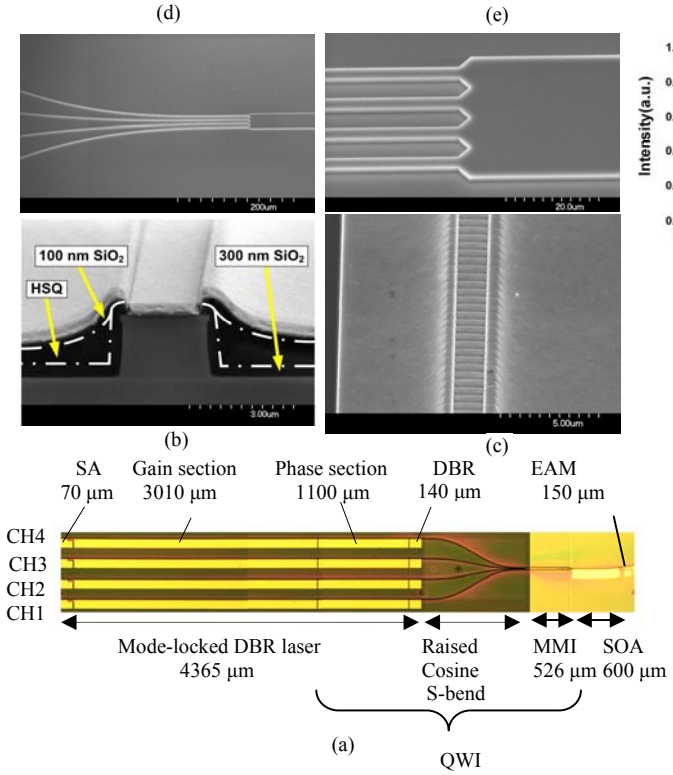

Fig.1 (a) Optical microscope picture of the device;(b) scanning electron microscope (SEM) picture of cross section of the ridge waveguide, (c) surface etched 3-order grating, (d) raised cosine S-bend, and (e) MMI.

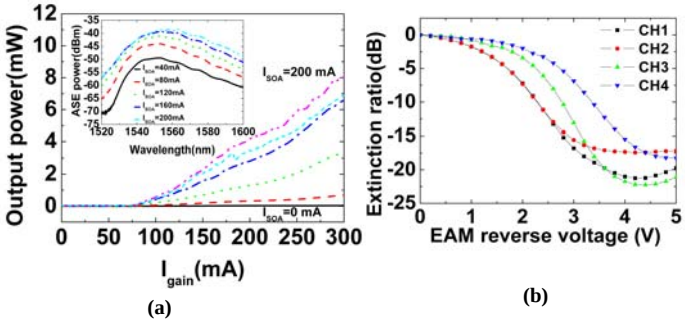

Fig.2 (a)Typical gain section L-I curves from the EAM side under SOA bias condition from 0 to 200 mA, in 40 mA steps from bottom to top and all other sections open, ASE spectra (inset); (b) EAM DC extinction behaviours of the 4-channels .

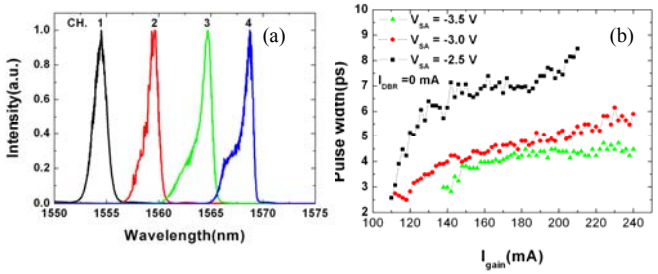

Fig.3 (a) 4-channel lasing spectra from EAM facets at I_{gain}=220 mA, I_{DBR}=0 mA V_{SA}= -3 V, and I_{SOA}=200 mA; (b) Measured pulse width vs. I_{gain} for V_{SA} = -2.5, -3, and -3.5 V respectively with I_{DBR}=0 mA, I_{SOA}=200 mA, phase and EAM sections left floating.

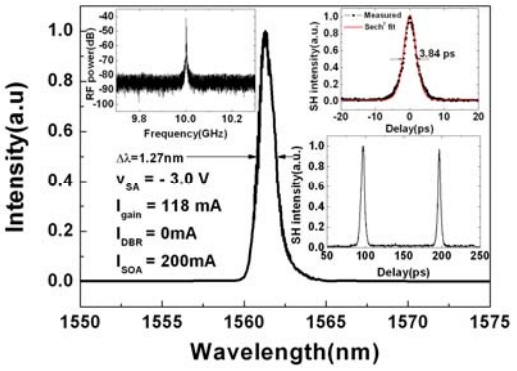

Fig.4 Optical spectrum, corresponding RF spectrum (left inset) and autocorrelation trace (right inset) for I_{gain} = 118 mA, I_{DBR} = 0 mA, I_{SOA} =200 mA, phase and EAM sections left floating, and V_{SA}= -3 V.

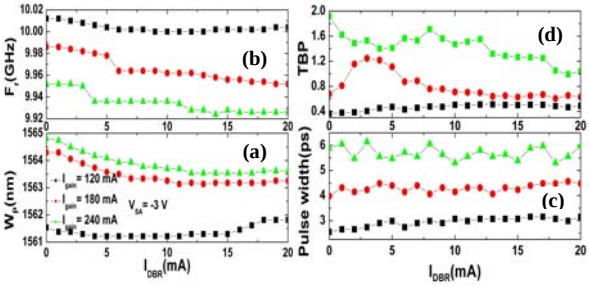

Fig. 5 (a)Emission peak wavelength (W_P), (b) pulse repetition frequency (Fr), (c) pulse width, and (d) TBPs vs. I_{DBR} for I_{gain} = 120, 180, and 240 mA while V_{SA}= -3.0 V, I_{SOA}=200 mA and all other sections left floating.